CrystEngComm

Accepted Manuscript

ROYAL SOCIETY OF CHEMISTRY

www.rsc.org/crystengcomm

Cite this: DOI: 10.1039/c0xx00000x

www.rsc.org/xxxxxx

ARTICLE TYPE

Metal Organic Framework (MOF) Micro/Nanopillars

Arben Kojtari,[1] Patrick J. Carroll,[2] and Hai-Feng Ji*[1]

Received (in XXX, XXX) Xth XXXXXXXXX 20XX, Accepted Xth XXXXXXXXX 20XX
DOI: 10.1039/b000000x

In this work, we report the realization of MOF-based micro/nanopillars, a new generation of MOF structures, prepared from surface-assisted self-assembly processes at room temperature. Cu(BTC)·3H2O and Zn(ADC)·DMSO were used as two model systems to demonstrate the formation of vertical MOF pillars on gold surfaces.

Metal-organic frameworks (MOFs) are porous, three-dimensionally linked coordination network materials that are composed of metal ions and organic molecules.[1,2] MOFs have exceptionally high specific surface areas and chemically tunable structures, which make them excellent materials for storage, purification, and separations of gases,[3] as well as for drug release/delivery,[4] heterogeneous catalysis,[5] and sensing.[6] Due to their unique inorganic–organic hybrid nature and porous structures at the nanometer scale, MOFs are rich in fundamental properties that promise new revolutionary device concepts. The vast majority of the studies in the past focused on the rational design, synthesis, characterization, and applications of MOFs in their micro-sized cubic crystals obtained from traditional MOF synthesis reactions, where the material is crystallized in solution. Recently, however, 2D films of MOFs (known as surface mounted metal-organic frameworks, or SURMOFs) and 1D micro/nanostructures, and MOF-based devices are gaining more interest due to potential in the fabrication of device coatings. However, most designs previously described require functionalized self-assembled monolayers to mediate attachment of the MOF to the surface covalently.

2D MOF thin films and coatings have been prepared from a variety of methods and interface types[7] which can be processed into integrated devices. These have yielded polycrystalline thin films,[8] SURMOF crystalline nanofilms,[9] MOF-coated silicon nanowires,[10] patterned growth,[11] and single crystal arrays.[12] Recently, 1D nanowire structures of MOFs have emerged.[13,14] However, a key barrier to wide-scale integration of functional 1D nanostructures into devices is the difficulty of forming efficient and programmed contacts between nanostructures and substrates with high reproducibility. One approach to mass-produce 1D nanowire arrays is to fabricate vertically oriented nanopillars.

Research on vertically oriented micro/nanopillar[15] is another rapidly growing area in the last decade because of the unique orientation of pillars and their easy-of-use for wide applications, such as photonic devices, cell growth and imaging,[16] antireflection,[17] light trap,[18] battery,[19] laser,[20] photodetector,[21] photovoltaics,[22] light-emitting diodes,[23] surface-enhance Raman spectroscopy (SERS) signal enhancing,[24] drug delivery,[25] sensors,[26] and enhanced selective catalysis.[27] One end of each micro/nanopillar is mechanically connected to the surface when the micro/nanopillars are fabricated. The uniqueness and advantage of the micro/nanopillar technique is that the structures are directly connected to the surface by being grown in place without the addition of a SAM coating to facilitate attachment. Micro/nanopillars are generally made of metals, silicon, oxides, and polymers, but the development of non-hybrid MOF pillar structures has remained absent from research studies. It has been expected that when pillars are made of highly porous materials such as MOFs, the porous micro/nanopillars can expand the applications of pillars into unique areas of photonics, surface catalysis, surface gas adsorption and purification, optoelectronic, drug delivery, and absorption-based sensing etc. In this paper, we demonstrate the first example of the growth of vertical MOF micro/nanopillars on surfaces from a surface-assisted method. The fabrication process involves a bottom-up method via an evaporation technique on chosen substrates to yield self-assembled pillar arrays. This method allows the MOF micro/nanopillars to have controllable interconnection of the micro/nanopillar devices through a vertical integration process using no lithography. This process meets industry requirements of low cost and high throughput, and offers significant advantages over transfer printing or pick-and-place methods to prepare nanowire based devices.

As seen in Figure 1A, mixing 500 µL of 3 mM 1,3,5-benzenetricarboxylic acid (BTC) and 500 µL of 30 mM $CuSO_4·5H_2O$ on gold surfaces yielded micro-sized $Cu(BTC)·3H_2O$ pillars with hexagonal cross-sections that were vertically oriented on the surface. Typical lengths ranged from 100-200 µm and diameters 20-50 µm when total crystallization time reached 24 hours. As evaporation time is extended both the diameter and the length of the micropillars increase. A similar result can be achieved by increasing the starting volume of both metal ion and ligand solutions used. This makes this class of pillar system ideal for tunable growth of MOF pillars.

In order to achieve nanopillar growth on gold substrates with substantially higher surface density, a modified procedure was utilized with success. 50 mg of BTC ligand was partially

dissolved in 10 mL of distilled water and stirred for 15 minutes at room temperature. The saturated solution was then filtered and 8 mL of the filtrate was added to a clean 20 mL vial. To this, 8 mL of a 30 mM $CuSO_4 \cdot 5H_2O$ solution was mixed with the saturated/filtered BTC solution. . Gold substrates were pretreated using single-second exposure to aqua regia solution as a wet-etching technique or wet physical abrasion of the surfaces. The latter technique worked more consistently in facilitating nanopillar growth, thus the results are described here. Surface growth is noticeable in less than 1 hour after initiation. Even after 30 minutes, a thin-film could be observed with the naked eye on the gold substrate. By 3 hours, samples have shown dense growth of a MOF nanopillar forest (Figure 1B). In typical experiments, substrates were removed after 3 hours and gently washed in distilled water baths and dried prior to surface characterization. $Cu(BTC) \cdot 3H_2O$ nanopillars prepared by this method were characterized having lengths typically in 10-40 μm but diameters in the nanometer range. The modified procedure allowed $Cu(BTC) \cdot 3H_2O$ to nucleate at more locations on the gold surface to facilitate the growth of nanopillars at high density.

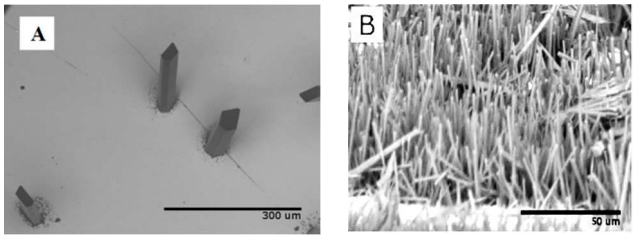

Fig. 1 (a) SEM image of $Cu(BTC) \cdot 3H_2O$ crystals fabricated on gold substrates over 24 hours. Single crystal vertical micropillars were prepared by mixing 500 μL of 3 mM BTC and 30 mM $CuSO_4 \cdot 5H_2O$ solutions. (b) SEM images of dense $Cu(BTC) \cdot 3H_2O$ nanopillar forest grown on gold substrates. Samples were prepared by mixing a saturated BTC solution along with 30 mM $CuSO_4 \cdot 5H_2O$ in equal volume quantities using wet physical abrasion of gold surfaces.

Zn(ADC)·DMSO pillar synthesis yielded crystals in similar fashion and the SEM images are shown in Figure S2 and S3 in the supplemental information.

Both MOF systems efficiently produced epitaxial growth of nano/micropillars on gold substrates. It should be noted that pillar growth is not influenced by the order of addition of the solutions. As controls, dissolved ligand solutions were allowed to dry on substrates to yield no ordered growth. Although pillars were mostly oriented perpendicular to the plane of the substrate, some of the pillars crystallized have variable tilt angles.

Single-crystal data and refinement parameters for both $Cu(BTC) \cdot 3H_2O$ and Zn(ADC)·DMSO systems are summarized in Table S1 in the supplemental information. The XRD study revealed the two-dimensional layers exhibited in the $Cu(BTC) \cdot 3H_2O$ system. Structure determination evidences that two of the three carboxylic acids of the BTC ligand are coordinated to the Cu^{2+} ion and forms zig-zag chains that are linked via hydrogen-bonding, which is facilitated by the third uncoordinated carboxylic acid and coordinated water molecules (Figure 2). Three water molecules (O7, O8, and O9) are coordinated to the distorted penta-coordinate copper geometry. The geometry is Jahn-Teller distorted to what appears to be a square-base pyramidal coordination geometry with O2 and O3 from the carboxylic acids of the BTC ligand and O7 and O9 of the water molecules to form the base of the square pyramid, as well as O8 coordinated axially. The geometry parameter τ, a measure of trigonality of a penta-coordinate system, was calculated using the calculation previously described as $\tau = (\beta - \alpha) / 60$ with angles used from the crystallographic data.[28] The calculated index value $\tau = 0.13$ indicates that the geometry around the five-coordinate Cu^{2+} metal is a slightly-distorted square-base pyramidal geometry rather than a trigonal bipyramidal geometry.

The layers of the coordination crystal are stacked on one-another, however, they do so unevenly. Figure 2B confirms that the 2D layers of $Cu(BTC) \cdot 3H_2O$ are held together not only by hydrogen-bonding, but parallel-displaced π-π stacking. The distance between the planes of the offset aromatic rings was measured to be 3.435 Å with a 15.6° angle displacement. The $Cu(BTC) \cdot 3H_2O$ sheets are layered to form three-dimensional architecture that contains water molecule channels that run the length of the crystal lattice. It is believed that the stability of the 3D structure relies on both intersheet hydrogen bonding of the copper-coordinated water molecules the π-π stacking of the BTC ligands.

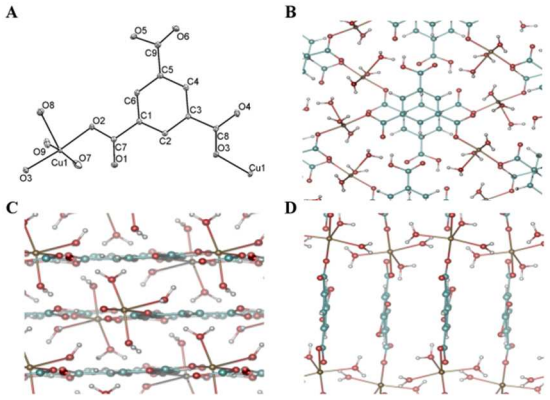

Fig. 2 $Cu(BTC) \cdot 3H_2O$ crystallographic representations (a) ORTEP illustration of the crystal structure with 50% probability ellipsoids. Packing structures (b) view along [100], (c) [010], and (d) [001] crystallographic planes. Coordination of BTC ligands to Cu^{2+} metals is responsible for one-dimensional polymeric growth of MOF system. Copper (bronze), carbon (cyan), oxygen (red), and hydrogen (white) atoms are shown.

Structure determination reveals that the Zn(ADC)·DMSO system shows a three-dimensional coordination framework that is highly linear along chains and lacking the presence of any hydrogen-bonding elements that could stabilize the MOF (Figure 3). Each Zn^{2+} ion is hexa-coordinated with four ADC ligands coordinating axially and the oxygens of two DMSO molecules coordinating equatorially to form a virtually undistorted octahedral geometry around the metal center. Each ADC ligand is coordinated to four Zn^{2+} ions, with the metal ions running linearly through the crystal structure with a distance of 3.654 Å. The crystal structure exhibits a herringbone packing arrangement of the ADC ligands with a interplane distance of 6.781 Å. The large distance between ADC ligands along the a-axis indicates that π-π stacking is not a contributing factor in stabilizing the 3D architecture, but rather ligand-metal coordination primarily.

Edge-to-face π-π stacking, which is common in the herringbone arrangement, was also absent within the structure. It should be noted that the single crystal study of Zn(ADC)·DMSO shows a disordered sulfur atom in DMSO. The positional disorder displaying variance of DMSO *O*-coordination to the Zn^{2+} center two positions arises from the disorder in crystal growth.

The crystal structure for this system also reveals small pores within the lattice of Zn(ADC)·DMSO. The smallest distance between ADC ligands coordinating to the same Zn^{2+} center was measured to be 3.837 Å, which could accommodate certain small molecules for separations and sensing applications. We believe that ultramicroporous materials are required for high specificity and sensitivity in the aforementioned applications described.

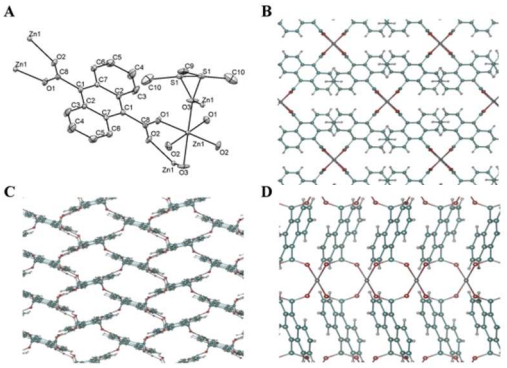

Fig. 3. Zn(ADC)·DMSO crystallographic representations (a) ORTEP illustration of the crystal structure with 50% probability ellipsoids. Packing structures (b) view along [100], (c) [010], and (d) [001] crystallographic planes. Coordination of ADC ligands to Zn^{2+} metals is responsible for three-dimensional polymeric growth of MOF system. Zinc (grey), carbon (cyan), oxygen (red), and hydrogen (white) atoms are shown. Disordered DMSO molecules are omitted for clarity.

The MOF nanopillars prepared in this work can be made in large quantities at a low cost due to the facile self-assembling method. This makes the method a viable option for preparing nanopillar-based devices or coatings.

In conclusion, vertical crystalline micro/nanowires of Cu(BTC)·3H_2O and Zn(ADC)·DMSO were synthesized and characterized in this work. The crystal structures of these MOF pillars are different from those prepared in bulk powder solutions, suggesting the surface does contribute to the growth of the crystals. The novel and facile approach for micro/nanopillar synthesis allows rapid pillared growth with high crystallinity of the MOF systems presented. Currently we are also investigating the nanopillar formation mechanism, the porosity and stability of MOF nanopillars, and whether the formation of these nanopillars can be controlled with the use of SAMs to pattern crystal growth by blocking the accessible gold surface.

For the past ten years, synthesis of nanopillars on substrates has revealed a wealth of unique magnetic, electrical, and optical properties. Being porous, the MOF nanopillars bring more new functions into play. These surfaces may be used for unique porous nanopillar based devices, such as catalyst based electrodes, catalytic reaction in microfluidic chips, high surface area electrode materials in electrochemical energy storage, fluorescence and photonic materials, sensors etc. We will investigate these possible applications and the results will be published in due courses.

ACKNOWLEDGMENT Support for this work was provided by the National Science Foundation (No. DMR-1104835)

Notes and references

[1]Department of Chemistry, Drexel University, Philadelphia, PA 19104 *the United States. Fax: 01-215-895-1265; Tel: 01-215-895-2562; E-mail:* hj56@drexel.edu [2] U. Penn. X-ray Crystallography Facility, University of Pennsylvania Philadelphia, PA 19104

1 O. Delgado-Friedrichs, M. O'Keeffe, and O. M. Yaghi, *Phys. Chem. Chem. Phys.*, 2007, **9**, 1035.
2 R. J. Kuppler, D. J. Timmons, Q.-R. Fang, J.-R. Li, T. a. Makal, M. D. Young, D. Yuan, D. Zhao, W. Zhuang, and H.-C. Zhou, *Coord. Chem. Rev.* 2009, **253**, 3042.
3 K. Sumida, S. Horike, S. S. Kaye, Z. R. Herm, W. L. Queen, C. M. Brown, F. Grandjean, G. J. Long, A. Dailly, J. R. Long, *Chem. Sci.* 2010, **1**, 184.
4 A. C. McKinlay, R. E. Morris, P. Horcajada, G. Férey, R. Gref, P. Couvreur, and C. Serre, *Angew. Chem. Int. Ed.* 2010, **49**, 6260.
5 a) J. Lee, O. K. Farha, J. Roberts, K. Scheidt, S. T. Nguyen, and J. T. Hupp, *Chem. Soc. Rev.* 2009, **38**, 1450. b) D. M. Robinson, Y. B. Go, M. Mui, G. Gardner, Z. Zhang, D. Mastrogiovanni, E. Garfunkel, J. Li, M. Greenblatt, G. C. Dismukes, *J. Amer. Chem. Soc.* 2013, **135**, 3494.
6 K. Sumida, D. L. Rogow, J. A. Mason, T. M. McDonald, E. D. Bloch, Z. R. Herm, T.-H. Bae, and J. R. Long, *Chem. Rev.* 2012, **112**, 724.
7 D. Bradshaw, A. Garai, and J. Huo, *Chem. Soc. Rev.* 2012, **41**, 2344.
8 A. Huang, H. Bux, F. Steinbach, and J. Caro, *Angew. Chem. Int. Ed.*, 2010, **49**, 4958.
9 G. Xu, T. Yamada, K. Otsubo, S. Sakaida, and H. Kitagawa, *J. Amer. Chem. Soc.*, 2012, **134**, 16524.
10 N. Liu, Y. Yao, J. J. Cha, M. T. McDowell, Y. Han, and Y. Cui, *Nano Res.*, 2011, **5**, 109.
11 J. Zhuang, J. Friedel, and A. Terfort, *Beil. J. Nanotech.* 2012, **3**, 570.
12 C. Carbonell, I. Imaz, and D. Maspoch, *J. Amer. Chem. Soc.*, 2011, **133**, 2144.
13 S.-M. Hu, H.-L. Niu, L.-G. Qiu, Y.-P. Yuan, X. Jiang, A.-J. Xie, Y.-H. Shen, and J.-F. Zhu, *Inorg. Chem. Comm.* 2012, **17**, 147.
14 K. M. L. Taylor, W. J. Rieter, and W. Lin, *J. Amer. Chem. Soc.*, 2008, **130**, 14358.
15 J. M. Spurgeon, K. E. Plass, B. M. Kayes, B. S. Brunschwig, H. a. Atwater, and N. S. Lewis, *Appl. Phys. Lett.*, 2008, **93**, 032112.
16 C. Xie, L. Hanson, Y. Cui, and B. Cui, *Pro. Nat. Acad. Sci.* 2011, **108**, 3894.
17 X. Li, J. Li, T. Chen, B. K. Tay, J. Wang, and H. Yu, *Nano. Res. Lett.*, 2010, **5**, 1721.
18 Z. Fan, R. Kapadia, P. W. Leu, X. Zhang, Y.-L. Chueh, K. Takei, K. Yu, A. Jamshidi, A. A. Rathore, D. J. Ruebusch, M. Wu, and A. Javey, *Nano Lett.*, 2010, **10**, 3823.
19 L. Ji, Z. Tan, T. Kuykendall, E. J. An, Y. Fu, V. Battaglia, and Y. Zhang, *Energy & Environ. Sci.*, 2011, **4**, 3611.
20 M.-H. Lo, Y.-J. Cheng, H.-C. Kuo, and S.-C. Wang, *Appl. Phys. Exp.* 2011, **4**, 022102.
21 K. J. Chen, F. Y. Hung, S. J. Chang, and S. J. Young, *Mat. Trans.* , 2009, **50**, 922.
22 A. Santos, P. Formentín, J. Pallarés, J. Ferré-Borrull, and L. F. Marsal, *Solar Energy Mat. Solar Cells,* 2010, **94**, 1247.
23 D.-W. Jeon, W. M. Choi, H.-J. Shin, S.-M. Yoon, J.-Y. Choi, L.-W. Jang, and I.-H. Lee, *J. Mat. Chem.*, 2011, **21**, 17688.
24 J. D. Caldwell, O. Glembocki, F. J. Bezares, N. D. Bassim, R. W. Rendell, M. Feygelson, M. Ukaegbu, R. Kasica, L. Shirey, C. Hosten, and C. E. T. Al, *ACS Nano*, 2011, 4046–4055.
25 A. K. Shalek, J. T. Robinson, E. S. Karp, J. S. Lee, D.-R. Ahn, M.-H. Yoon, A. Sutton, M. Jorgolli, R. S. Gertner, T. S. Gujral, G. MacBeath, E. G. Yang, and H. Park, *Proc. Nation. Acad. Sci.*, 2010, **107**, 1870.
26 C. Shin, W. Shin, and H.-G. Hong, *Electrochim. Acta*, 2007, **53**, 720.
27 F. Zaera, *Chem. Soc. Rev.* 2012, **42**, 2746.
28 A. W. Addison and G. C. Rao, T. N.; Reedijk, J.; van Rijn, J.; Verschoor, *J. Chem. Soc. Dal. Trans.* 1984, 1349.